

Actin polymerization in a thermal gradient

Andrew Pomerance¹, Jermev Matthews², Matthew Ferguson^{1,3}, Jeffrey S. Urbach⁴, Wolfgang Losert^{*1}

1 Department of Physics, Institute for Physical Science and Technology, and Institute for Research in Electronics and Applied Physics, University of Maryland, College Park, Maryland 20742, USA; Email: wlosert@glue.umd.edu

2 Department of Chemical Engineering, University of Maryland, College Park, MD 20742, USA

3 Laboratory of Integrative and Medical Biophysics/National Institute of Child Health and Human Development/NIH, Bethesda, MD 20892, USA

4 Department of Physics, Georgetown University, Washington, DC 20057, USA

Summary: Actin polymerization was studied as a function of temperature and in controlled thermal gradients. In the absence of a thermal gradient, we observe a polymerization transition with a temperature increase of less than 10K, and we verify that microrheology provides a local measure of the polymerized fraction. Both of these results are in good agreement with prior observations. Thermal gradients allow us to generate polymerization gradients. This polymerization gradient induces motion in embedded microspheres that is not seen in control samples.

Keywords: Microrheology, actin, thermal gradient, polymerization transition

Introduction

The polymerization dynamics of actin filaments play a central role in the rapid cytoskeletal rearrangements necessary for cell motility and maintaining cell shape^{1,2}. Together with microtubules and intermediate filaments, actin is a component of the cytoskeleton, the dynamic scaffolding inside each cell. Actin filaments can grow or shrink, and in the process can exert forces on surrounding objects, a mechanism that is used by e.g. *Lysteria* bacteria who propel themselves by polymerizing actin in their host cell³. *In vivo*, the dynamic rearrangements of actin are controlled by a myriad of helper proteins that nucleate, cross-link, and cap growing actin filaments. *In vitro*, individual actin monomers (globular actin or G-actin) polymerize completely in the presence of K⁺ or Mg²⁺ to a double stranded chain of actin (filamentous actin or F-actin). For a review of actin properties see Sheterline *et al.*⁴.

Two of the simplest ways to control actin polymerization are by control of concentration or temperature. Systematic studies of actin polymerization as a function of

concentration have shown a polymerization transition above a critical concentration of G-actin⁵. At physiological actin concentrations but low salt concentrations, the polymerization fraction can be controlled by temperature⁶. The polymerization fraction remains low until a floor temperature, T_p , where the polymerization fraction increases sharply over only 5-10 K with increasing temperature, until it reaches a maximum polymerization, T_{max} , beyond which further temperature increases may cause a decrease in the polymerized fraction. Based on these data, Niranjana et al.⁷ have developed a model of actin polymerization as a sequence of four steps – monomer activation, dimerization, trimerization, and elongation and mapped out the entropies and enthalpies of each step.

Our aim is to measure forces and polymer network inhomogeneities generated by polymerization gradients. The rapid change in polymerized fraction with temperature provides a powerful tool for spatial and temporal control of actin polymerization. Unlike actin concentration, temperature is an external variable that can be tuned rapidly and changed locally, and that can be accurately measured. Variations in temperature allow us to generate controlled changes in polymerization and to obtain polymerization gradients. Here, we show a calibration of our system and initial results on polymerization gradients generated by steep thermal gradients.

Materials and Methods

Actin preparation: G-actin solutions are prepared from rabbit muscle acetone powder, as described by Pardee and Spudich⁸. The actin is extracted from the acetone powder as described in Niranjana et al.⁹ with the following changes. After the first ultracentrifugation, the actin is homogenized in buffer A (4 mM Tris, 0.2 mM CaCl_2 , 0.2 mM disodium adenosine triphosphate, 0.005% NaN_3 , 0.5 mM dithiothreitol, adjusted with HCl (aq) to final pH 8.0 at 25.0 °C) and re-pelleted. After the second pelleting, the actin is homogenized and then dialyzed against buffer A at 4 °C with rapid stirring, for ≈ 96 h. G-actin is purified and concentrations are determined and adjusted as described by Niranjana et al.⁹ After purification, 9mM KCl is added to the sample, as well as 2 μm diameter carboxyl-modified polystyrene beads from Polysciences, Inc.

Pyrene Fluorescence assay: Pyrene-labeled actin fluoresces approximately ten-fold more strongly in the polymerized state than in the unpolymerized state. Therefore measurement of pyrene fluorescence is a sensitive assay for actin polymerization⁹⁻¹¹. Actin was dialyzed into buffer A. Its concentration was measured to be approximately 2 mg/mL and was then mixed 2:1 with 2 mg/mL 10% (molar) pyrene-labeled actin

resuspended from freeze dried powder into buffer A. This yields a final solution of 1.9g/L 3% (molar) pyrene labeled actin in Buffer A. The Pyrene-labeled actin (labeling stoichiometry of 0.3 – 0.8 pyrenes per actin monomer) was purchased from Cytoskeleton, Denver, CO. The sample was placed in a quartz cell with 0.3 cm path length and 50 μ l sample volume. Pyrene fluorescence was measured in an ISS PC1 photon counting spectrofluorometer, and the sample temperature was maintained by a Quantum Northwest Peltier stage to within 0.03 °C. Pyrene fluorescence was excited at 340nm, and data were collected at 386 nm.

Local polymerization measurement (microrheology): Local measurements of the viscoelastic properties can be used to characterize polymerization gradients of actin. We utilize particle-tracking microrheology¹², which has been used before in dilute actin networks¹³. We measure the motion of the beads using digital imaging and particle tracking routines developed by Crocker, Grier and others, and described e.g. in Ref ¹². The limitations of such measurements are that the local environment of the beads may be different from the typical environment and that the bead may perturb the local environment.

Experimental setup: Actin samples were placed between two fused quartz microscope slides with a 75 μ m mylar spacer between them as shown in schematic of the experimental setup in Figure 1. Quartz slides were used because borosilicate glass leaches ions into the solution, which induces actin polymerization¹⁴. Fused quartz also has a much higher thermal conductivity than glass¹⁵, which makes it better suited for temperature gradient experiments. The temperature is controlled by two copper blocks connected to separate water baths, which are independently controlled to within 0.1 K. The actin-containing sample slide is placed under the two thermal blocks, which are spaced two millimeters apart (see figure 1). For uniform temperature experiments, the two blocks are set to the same temperature. In most temperature gradient experiments, the temperature of the hot water bath is set to 40 °C, just below the denaturation temperature of actin, and the cold water bath is set to 4 °C. The resulting temperature gradient inside the sample cell was measured with a thermocouple glued between two quartz slides, which is moved slowly (~1 μ m/s) through the gradient. Due to gradients at the contact to the sample cell, and within the cell walls, the measured thermal gradient inside the sample cell is 5 K/mm.

The actin sample is imaged on an inverted microscope. At 4x magnification, a time lapse camera with 6.7 μ m wide pixels and a frame time of 6 s/frame was used to image the

entire gradient. At 50x magnification (long working distance), a high speed camera with 12 μm pixels was used to image the sample for 63 seconds at 60 frames per second.

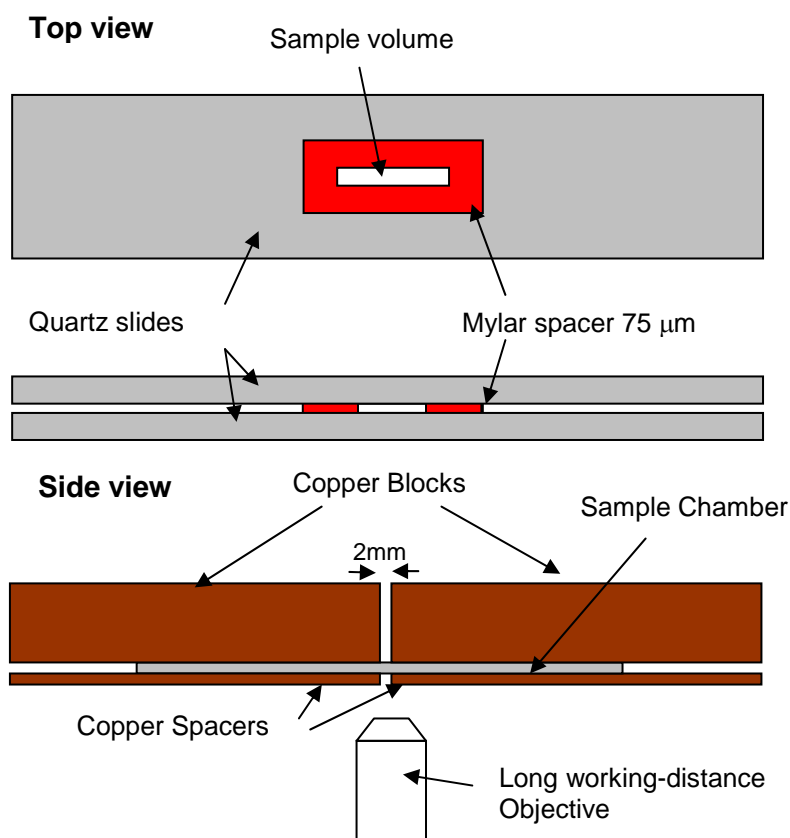


Figure 1: Experimental setup for controlled temperature and thermal gradient actin microrheology.

Temperature dependent actin polymerization

Measurements of materials properties in polymerization gradients require a local probe of polymerization such as microrheology. As a first step we have compared microrheology measurements with pyrene fluorescence measurements at different polymerized fractions. The fluorescence data are also compared to prior work⁷. To our knowledge, no microrheology measurements on partially polymerized networks have been carried out previously.

Pyrene Fluorescence: The sample was equilibrated at 4 $^{\circ}\text{C}$ in the spectrofluorimeter and 9mM KCl was then added and gently mixed into the sample. The temperature was stepped from 5 $^{\circ}\text{C}$ to 40 $^{\circ}\text{C}$ in 2 K steps. After all steps the sample was allowed to equilibrate for 30 minutes. The polymerization of the sample was determined from the maximum fluorescence intensity during that period, as shown in Figure 2. As shown in figure 3, the actin fluorescence did not equilibrate in 30 minutes in contrast to prior work

where 30 minutes was sufficient to equilibrate the sample⁷. This may be due to residual impurities in the pyrene labeled actin which, unlike the unlabeled actin, was used as purchased without further purifications. In order to ensure that addition of microspheres did not affect actin polymerization thermodynamics, actin polymerization was also measured at two concentrations of microspheres, 0.01% and 0.1% by volume (figure 2). The addition of microspheres does not significantly affect the polymerization temperature at least for the lower concentration.

Bead tracking measurements: The same temperature change protocol and actin concentration was also used for particle tracking microrheology, except that samples were allowed to equilibrate for 45 minutes instead of 30 minutes. In addition to the KCl, 0.01% concentration by volume microspheres were added to the sample for particle tracking. The sample was then imaged with a 50x objective and every ten minutes, 4096 frames at a resolution of 640x480 pixels and 60 frames per second (yielding 2 minutes of video) were captured and analyzed. Approximately 100 particles were tracked per frame. A typical particle track is shown in Figure 4, and a typical averaged mean squared displacement (MSD) of all particles in an image sequence as a function of time is shown in Figure 5. As the actin network polymerizes, trapped microspheres transition from diffusive to sub-diffusive motion. The MSD over long timescales can be described well with a power law, i.e. $\Delta x^2 = Dt^\gamma$, with a diffusive exponent $\gamma < 1$ ¹². Earlier work showed that this diffusive exponent is sensitively dependent on the ratio of the radius of the microsphere a to cage size, a/ζ ¹⁶. Figure 6 shows γ vs. temperature for a representative experiment. The diffusive exponent was measured every ten minutes, so there are four or five measurements at each temperature, and all of these values are plotted. This result can be understood by generalizing the formula for the cage size of an actin gel, $c_s = \zeta = 0.3/\sqrt{c_A}$ [13], by replacing c_A , the concentration of actin as measured in mg/mL, with $C_{\text{eff}} = c_A * \phi$, where ϕ is the polymerization fraction. Thus, as ϕ increases from 0 to 1, the cage size decreases, trapping the particles more tightly. A major drop in the exponent occurs at approximately 10% polymerized fraction, where the cage size (estimated as described below) is on the order of the particle size. However, the diffusive exponent reaches a minimum around 25 °C, which indicates that the particles are most strongly caged at the temperature. This is consistent with pyrene fluorescence measurements by Niranjana *et al.*⁷ that indicate a higher polymerized fraction, i.e. the local bead tracking measurements are consistent with the global measure of polymerization provided by pyrene fluorescence.

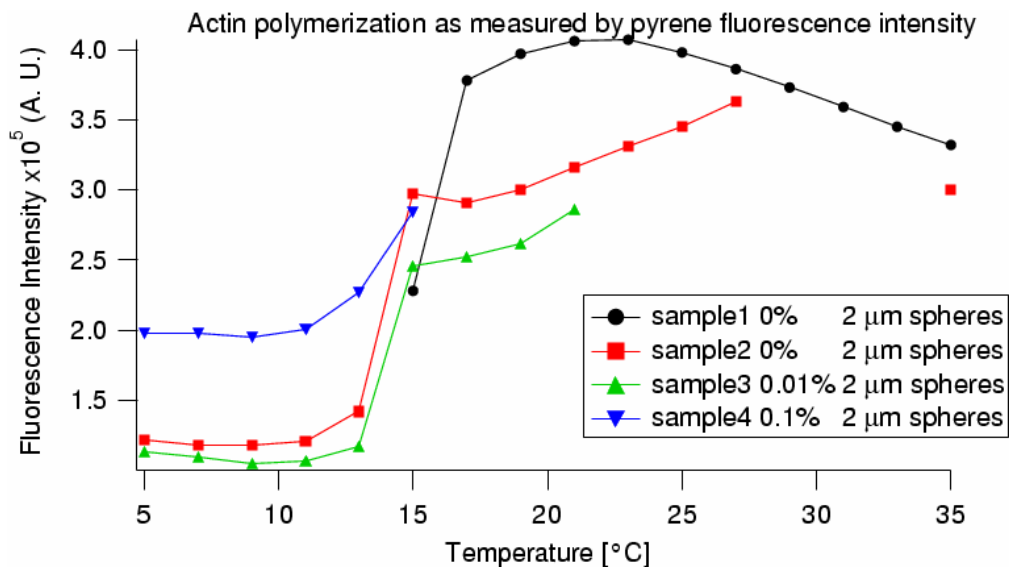


Figure 2: Fluorescence intensity vs temperature for 4 samples at 3 different 2 μm diameter microsphere concentrations. The sample was excited at 340 nm, and emission was measured at 386 nm. The polymerization transition occurs around 15°C, without or with microspheres added at low concentrations. (For details see text)

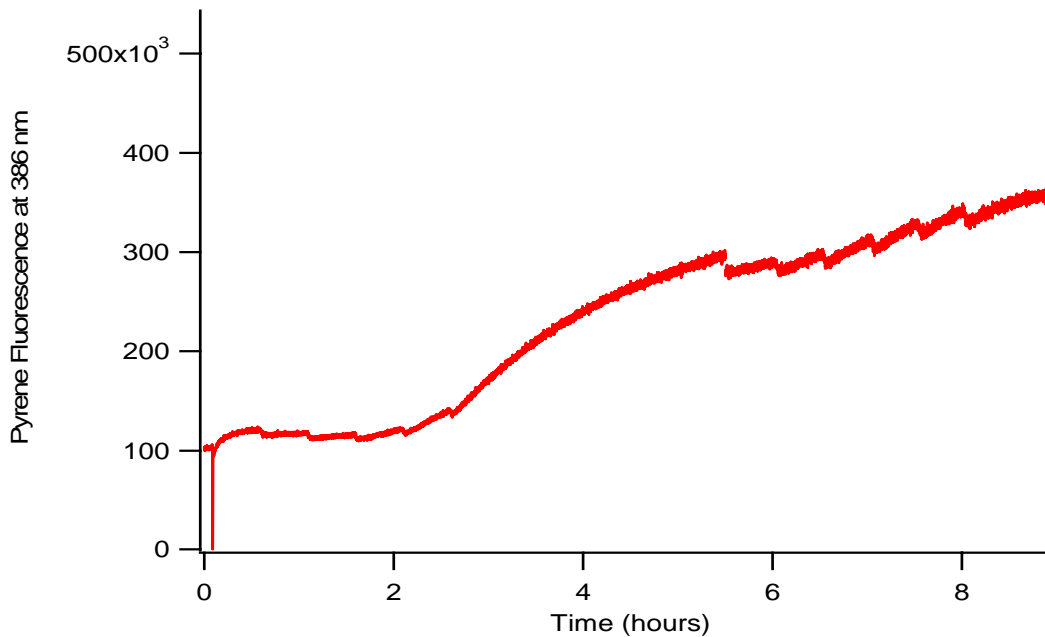


Figure 3: Pyrene fluorescence vs. time. Note that the fluorescence does not equilibrate in 30 minutes, possibly due to impurities introduced with the labeled actin that was used as purchased without further purification.

The MSD is also used to estimate the complex viscoelastic modulus $G^*(\omega)$ of the surrounding actin network by a generalized Stokes-Einstein relation,

$$G^*(\omega) = \frac{k_B T}{\pi a i \omega \langle \Delta x^2(\omega) \rangle}$$

where $\langle \Delta x^2(\omega) \rangle$ is the Fourier transform of the mean square displacement $\langle \Delta x^2(t) \rangle$ measured from the particle motion¹⁷. This approach assumes that the particle size a is much larger than the average cage size of the entangled actin network. This is the case at a polymerization fraction ϕ of 1 where the average cage size is $\zeta \sim 0.42 \mu\text{m}$ and should be a good approximation down to $\phi \sim 10\%$. This technique may not be sensitive to network inhomogeneities, and neglects the perturbation of the bead on the network (which may be important in a gradient as shown below). The viscoelastic moduli as calculated with the generalized Stokes-Einstein relation are plotted in figure 7. An important characteristic of these plots is the crossover frequency, which indicates at which frequency elastic behavior begins to dominate the low-frequency viscous behavior. This frequency is inversely proportional to the relaxation time of the network, which gives a rough indication of average polymer length. As shown in the figures, after the transition from viscous to soft elastic material, the crossover frequency moves to higher frequency at higher temperatures, which implies a shorter relaxation time. This indicates that the average chain length may be shorter at higher temperature. This may lead to a softening of the network, which is consistent with the higher diffusive exponent at higher temperature.

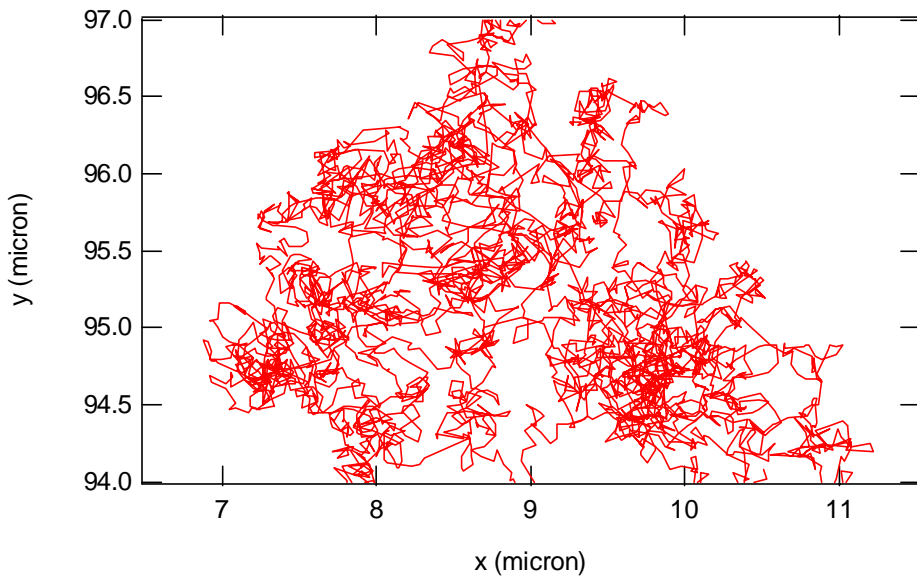


Figure 4: Sample particle track

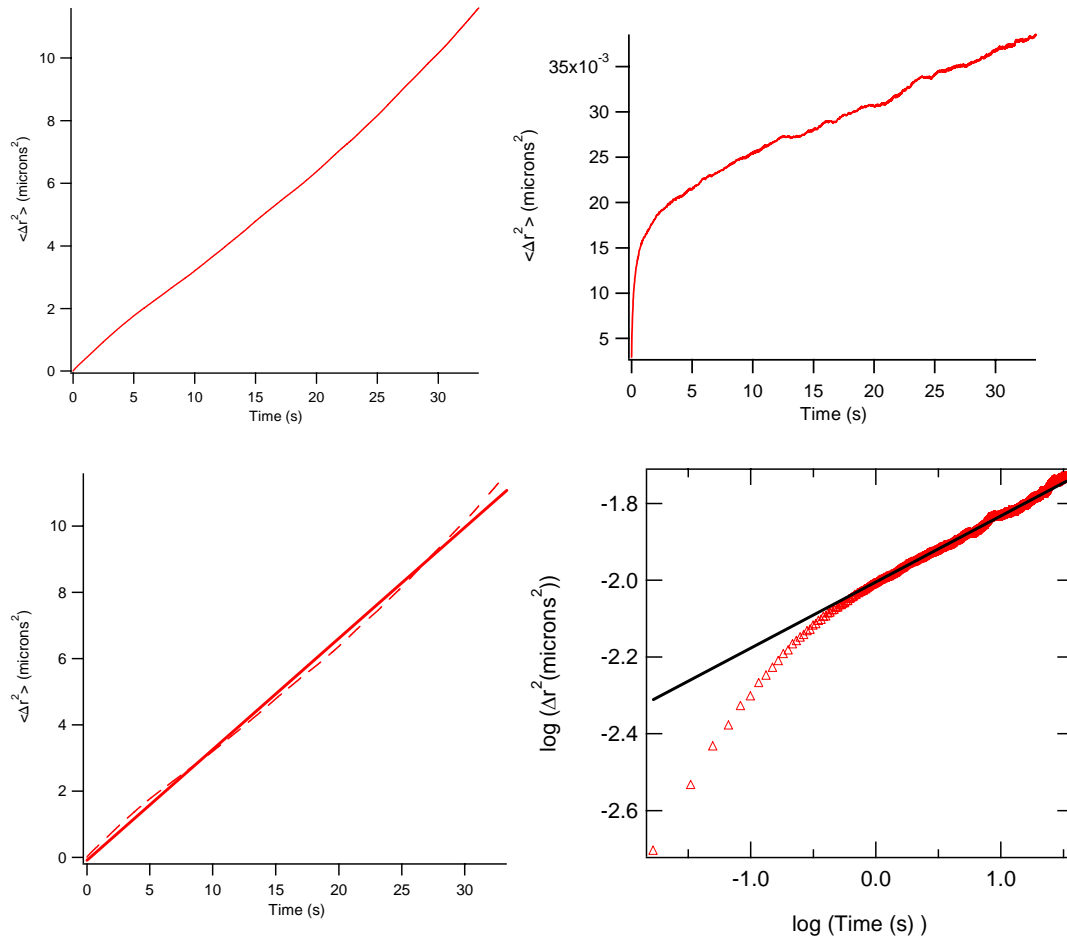


Figure 5: Mean squared displacement vs time for the unpolymerized case (top left) and polymerized case (top right). A linear fit (bottom left) in the unpolymerized case gives the diffusion constant of beads in actin solution, whereas a linear fit on a log-log plot (bottom right) of the polymerized case gives the diffusive exponent.

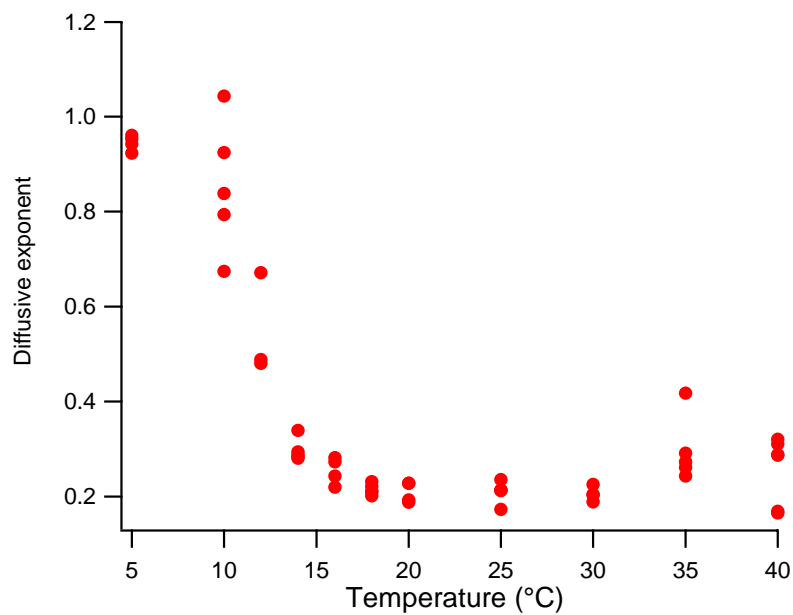


Figure 6: Diffusive exponent γ as a function of temperature for one run. See text.

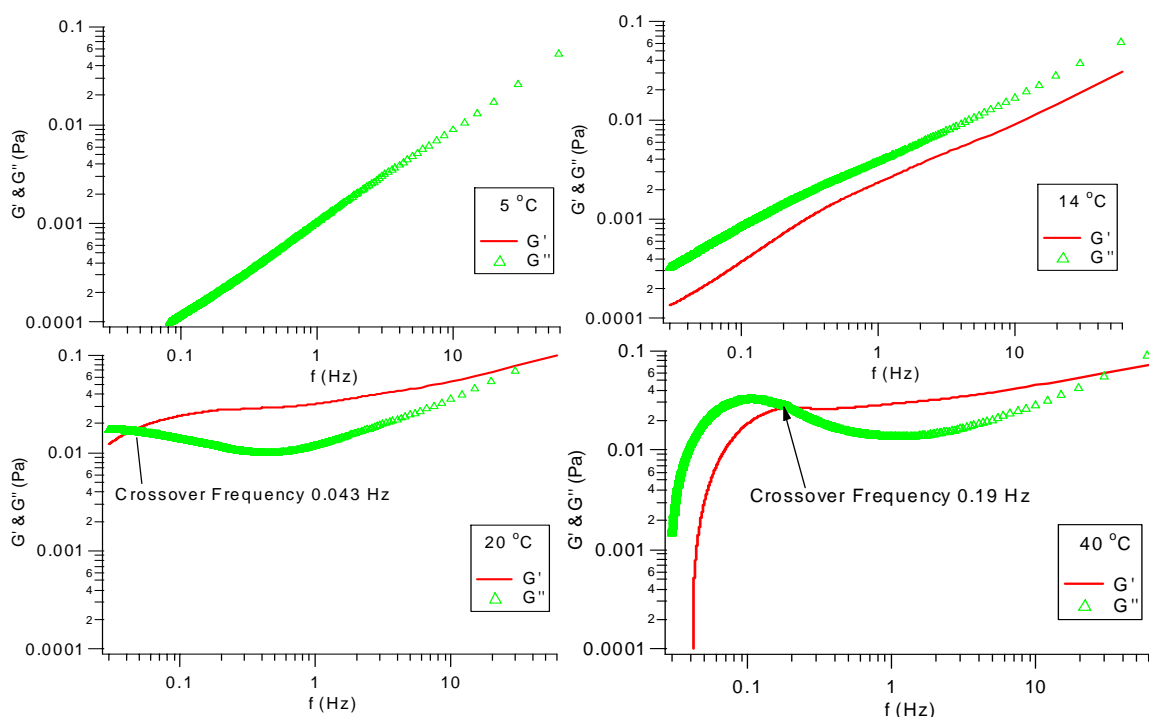


Figure 7: Complex viscoelastic moduli as a function of frequency, as calculated with the generalized Stokes-Einstein relation. As can be seen, the sample makes a transition from purely viscous behavior at 5 C in (a), to viscoelastic behavior at 14 C in (b). As the temperature is further increased to 20 C in (c), the crossover frequency is very low, indicating longer polymer chains. Finally, as the sample temperature is increased to 40 C in (d), the crossover frequency increases indicating slight depolymerization of the network.

Actin in a Thermal Gradient

Having established the temperature dependence of the viscoelastic properties of actin gels at low salt concentrations, we placed actin samples in a temperature gradient. We used 3 mg/mL actin solutions because of the sharper polymerization transition with temperature, which should give a sharper polymerized front. We imaged the beads with a 4x objective and captured frames a 1/6 frames/second, in order to image the entire gradient and capture the slow kinetics of the system.

We observe a net flow of embedded microspheres in the direction from hot to cold. The speed of the flow is quite slow and fairly consistent in magnitude and direction from run to run, around 0.1 $\mu\text{m/s}$. Figure 7 shows the trajectories of particles moving through the thermal gradient in a typical experiment.

One explanation for the observed drift of particles is that the polymerization gradient of actin (generated by applying a thermal gradient) exerts forces on the particle.

Before focusing on that mechanism, we discuss mechanisms unrelated to forces generated by the polymerization gradient: global Gel swelling may cause bead motion, or the actin gel could be relaxing slowly due to pressure differences caused by an imbalance between the copper blocks that are pressed against the sample for good thermal contact (see Figure 1). The consistent speed and direction of the motion of particles is evidence against such a mechanism, though further experiments will be carried out to rule out this possibility. Convection generated by thermal gradients is a possible source of motion, but using a thin sample minimized convection, and in control experiments with beads in water in a thermal gradient we observe no net flow.

We can estimate the average force exerted by each filament: The average number of filaments pushing on a bead can be estimated as $N = \pi r^2 / \zeta^2$, where r is the radius of the particle and ζ is the cage size of the polymer. At 3 mg/mL, the cage size $\zeta = 0.34 \mu\text{m}$. Therefore, the maximum total number of filaments pushing on a 2 micron diameter bead is approximately 27. However, since most of the sample is less than fully polymerized, N is lower than 27. Since this is a low Reynolds number system, we can equate the force produced by the actin gel with the viscous drag, which is given by $F_{drag} = 6\pi\eta r v = N F_{poly}$. Using $\eta = 10^{-3} \text{ Pa}\cdot\text{s}$ and $v = 0.2 \mu\text{m/s}$, this yields an estimate of $F_{poly} = 3.6\text{e-}3 \text{ pN}$ if the bead is moving in water. This is a lower bound estimate that ignores that the beads may be moving relative to the actin network.

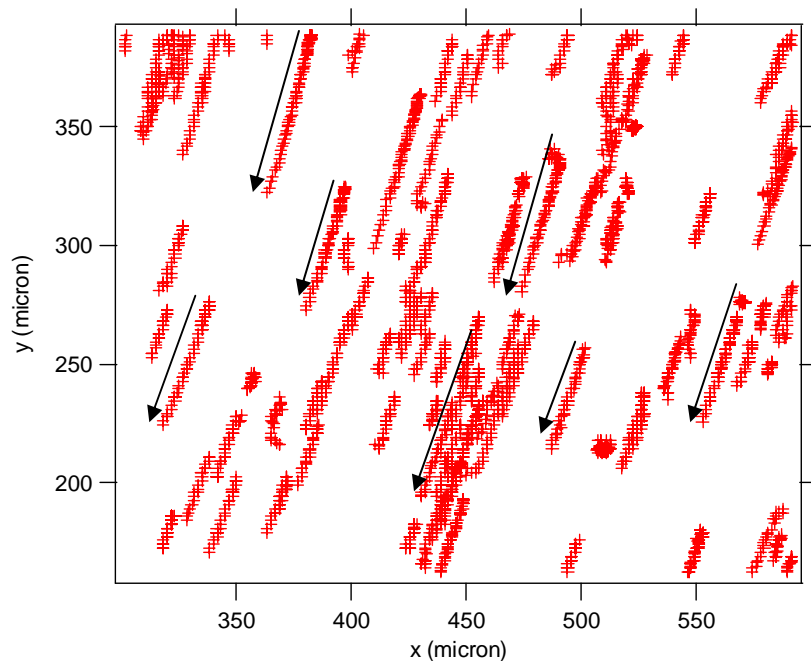


Figure 8: Sample particle tracks from a temperature gradient experiment. Particles moved in the direction indicated by the arrows. The hot side is at the top of the figure.

As a consistency check, we can calculate the maximum force a polymerizing actin network can exert using thermodynamic relations. The work done by a polymerizing actin filament is limited to the change in free energy of polymerization, $\Delta G = \Delta H_{prop} - T\Delta S_{prop}$. Using $\Delta H_{prop} = 138$ kJ/mol and $\Delta S_{prop} = 0.59$ kJ/mol-K [this should be ref. 7] at 300 K this yields $\Delta G = -29$ kJ/mol = $4.8e-20$ J/monomer. Assuming all the work goes to pushing a bead, and using 4 nm as the size of an actin monomer, this yields $F_{poly} = 12$ pN/filament.

Conclusions and Discussion

We have carried out microrheology measurements of partially polymerized actin networks across the temperature dependent polymerization transition. The local polymerization probes are consistent with bulk measures of the polymerized actin fraction.

We then used thermal gradients to generate gradients in the polymerized actin network. We find a slow drift of particles toward the less polymerized side of the sample. Various tests indicate that the drift is likely due to the polymerization gradient of actin, not due to other mechanisms.

There are several possible mechanisms by which a polymerization gradient could exert forces and push beads to the weaker region of the network: Actin monomers could be added to filaments preferentially in the hotter region of the sample with a denser filament network, and removed in colder regions, leading to a net treadmilling motion of the filaments or a global translation of the gel, which would entrain the trapped beads with it. On the other hand, the drift may be due to a process similar to impurity extrusion from growing crystal. The energy required to accommodate a bead increases with increasing network density; therefore, a gradient in network density could give rise to the forces that cause the beads to drift. In addition, the Soret effect, which is a concentration gradient generated by a thermal gradient¹⁸, may play a role, though the size or even sign of the resulting flux of beads in actin is unknown. Moreover, electrostatic effects may be important. Carboxyl groups on our bead surfaces are slightly negatively charged. Actin filaments in solution also carry a slight negative charge; therefore the beads may be extruded from higher density areas due to Coulomb interactions with the actin filaments. A systematic study to discern several of these gradient forces is underway.

Acknowledgements: We thank Sandra Greer and Jeff Forbes for sharing their expertise in

actin purification and polymerization. Special thanks to Jack Douglas for fruitful discussions in the design and interpretation of these experiments. Part of this work was supported by NIH Grant # 1-R21-EB-00328501.

- (1) Mogilner, A.; Oster, G. *Biophys. J.* **1996**, *71*.
- (2) Borisy, G. G.; Svitkina, T. M. *Curr. Cell Biol.* **2000**, *12*, 104.
- (3) Theriot, J. A.; Mitchison, T. J. *Nature* **1991**, *352*, 126-131.
- (4) Sheterline, P.; Clayton, J.; Sparrow, J. C. *actin*; Oxford Univ. Press: Oxford, U.K., 1998.
- (5) Alberts, B.; Johnson, A.; Lewis, J.; Raff, M.; Roberts, K.; Walter, P. *Molecular Biology of the cell*; Taylor & Francis: New York, 2002.
- (6) Greer, S. C. *J. Phys. Chem. B* **1998**, *102*, 5413-5422.
- (7) Niranjana, P. S.; Forbes, J. S.; Greer, S. C.; Dudowicz, J.; Freed, K. F.; Douglas, J. F. *J. Chem. Phys.* **2001**, *114*, 10573-10576.
- (8) Pardee, J. D.; Spudich, J. A. In *Methods in Enzymology: Structural and Contractile Proteins*; Cunningham, D. W. F. a. L. D., Ed.; Academic: New York, 1982; Vol. 85, p 164.
- (9) Niranjana, P.; Yim, P.; Forbes, J.; S., G.; Dudowicz, J.; Freed, K.; Douglas, J. *J. Chem. Phys.* **2003**, *119*, 4070-4084.
- (10) Cooper, J. A.; Walker, S. B.; Pollard, T. D. *J. Muscle Res. Cell Motil.* **1983**, *4*, 253.
- (11) Cooper, J. A.; Pollard, T. D. In *Methods in Enzymology: Structural and Contractile Proteins*; Cunningham, D. W. F. a. L. D., Ed.; Academic: New York, 1982; Vol. 85, p 182.
- (12) Gardel, M. L.; Valentine, M. T.; Weitz, D. A. In *Microscale Diagnostic Techniques*; Breuer, K., Ed.; Springer Verlag: Heidelberg, 2002.
- (13) Gardel, M. L.; Valentine, M. T.; Crocker, J. C.; Bausch, A. R.; Weitz, D. A. *Phys. Rev. Lett* **2003**, *91*, 158302.
- (14) Niranjana, P. S.; Forbes, J. G.; Greer, S. C. *Biomacromolecules* **2000**, *1*, 506-508.
- (15) Lide, D. *CRC Handbook of Chemistry and Physics*, 81st ed.; CRC Press: Boca Raton, 2000.
- (16) Wong, I. Y.; Gardel, M. L.; Reichman, D. R.; Weeks, E. R.; Valentine, M. T.; Bausch, A. R.; Weitz, D. A. *Phys. Rev. Lett* **2004**, *92*, 178101.
- (17) Mason, T. G.; Gang, H.; Weitz, D. A. *Journal of the Optical Society of America A* **1997**, *14*, 139.
- (18) Wiegand, S. *Journal of Physics: Condensed Matter* **2004**, *16*, R357-379.